Electromagnetically induced transparency and ultraslow optical solitons in a coherent atomic gas filled in a slot waveguide

Jin Xu and Guoxiang Huang*

State Key Laboratory of Precision Spectroscopy and Department of Physics, East China Normal University, Shanghai 200062, China

**gxhuang@phy.ecnu.edu.cn*

Abstract: We investigate the electromagnetically induced transparency (EIT) and nonlinear pulse propagation in a Λ-type three-level atomic gas filled in a slot waveguide, in which electric field is strongly confined inside the slot of the waveguide due to the discontinuity of dielectric constant. We find that EIT effect can be greatly enhanced due to the reduction of optical-field mode volume contributed by waveguide geometry. Comparing with the atomic gases in free space, the EIT transparency window in the slot waveguide system can be much wider and deeper, and the Kerr nonlinearity of probe laser field can be much stronger. We also prove that using slot waveguide ultraslow optical solitons can be produced efficiently with extremely low generation power.

OCIS codes: (020.1670) Coherent optical effects; (130.2790) Guided waves; (270.5530) Pulse propagation and temporal solitons.

References and links

1. M. Fleischhauer, A. Imamoglu, and J. P. Marangos, "Electromagnetically induced transparency: Optics in coherent media," Rev. Mod. Phys. **77**, 633-673 (2005).
2. L. V. Hau, S. E. Harris, Z. Dutton, and C. H. Behroozi, "Light speed reduction to 17 metres per second in an ultracold atomic gas," Nature. **397**, 594-598 (1999).
3. M. M. Kash, V.A. Sautenkov, A. S. Zibrov, L. Hollberg, G. R. Welch, M. D. Lukin, Y. Rostovtsev, E. S. Fry, and M.O. Scully, "Ultraslow group velocity and enhanced nonlinear optical effects in a coherently driven hot atomic gas," Phys. Rev. Lett. **82**, 5229-5232 (1999).
4. A. I. Lvovsky, B. C. Sanders, and W. Tittel, "Optical quantum memory," Nat. Photon. **3**, 706-714 (2009).
5. H. Zhang, X.-M. Jin, J. Yang, H.-N. Dai, S.-J. Yang, T.-M. Zhao, J. Rui, Y. He, X. Jiang, F. Yang, G.-S. Pan, Z.-S. Yuan, Y. Deng, Z.-B. Chen, X.-H. Bao, S. Chen, B. Zhao, and J.-W. Pan, "Preparation and storage of frequency-uncorrelated entangled photons from cavity-enhanced spontaneous parametric downconversion," Nat. Photonics **5**, 628-632 (2011).
6. H. N. Dai, H. Zhang, S.-J. Yang, T.-M. Zhao, J. Rui, Y.-J. Deng, L. Li, N.-L. Liu, S. Chen, X.-H. Bao, X.-M. Jin, B. Zhao, and J.-W. Pan, "Holographic storage of biphoton entanglement," Phys. Rev. Lett. **108**, 210501 (2012).
7. C. Ottaviani, D. Vitali, M. Artoni, F. Cataliotti, and P. Tombesi, "Polarization qubit phase gate in driven atomic media," Phys. Rev. Lett. **90**, 197902 (2003).
8. C. Hang, Y. Li, L. Ma, and G. Huang, "Three-way entanglement and three-qubit phase gate based on a coherent six-level atomic system," Phys. Rev. A **74**, 012319 (2006).
9. Y. Wu, and L. Deng, "Ultraslow optical solitons in a cold four-state medium," Phys. Rev. Lett. **93**, 143904 (2004).
10. G. Huang, L. Deng and M. G. Payne, "Dynamics of ultraslow optical solitons in a cold three-state atomic system," Phys. Rev. E. **72**, 016617 (2005).

#180953 - $15.00 USD Received 30 Nov 2012; revised 13 Jan 2013; accepted 15 Jan 2013; published 22 Feb 2013

11. S. Johnson, M. Ibanescu, M. Skorobogatiy, O. Weisberg, T. Engeness, M. Soljacic, S. Jacobs, J. Joannopoulos, and Y. Fink, "Low-loss asymptotically single-mode propagation in large-core OmniGuide fibers," Opt. Express **9**, 748-779 (2001).
12. S. Ghosh, J. E. Sharping, D. G. Ouzounov, and A. L. Gaeta, "Resonant optical interactions with molecules confined in photonic band-gap fibers," Phys. Rev. Lett. **94**, 093902 (2005).
13. S. Ghosh, A. R. Bhagwat, C. K. Renshaw, S. Goh, and A. L. Gaeta, "Low-light-level optical interactions with rubidium vapor in a photonic band-gap fiber," Phys. Rev. Lett. **97**, 023603 (2006).
14. P. S. Light, F. Benabid, F. Couny, M. Maric, and A. N. Luiten, "Electromagnetically induced transparency in Rb-filled coated hollow-core photonic crystal fiber," Opt. Lett. **32**, 1323-1325 (2007).
15. F. Benabid, P. Light, F. Couny, and P. Russell, "Electromagnetically-induced transparency grid in acetylene-filled hollow-core PCF," Opt. Express **13**, 5694-5703 (2005).
16. M. Bajcsy, S. Hofferberth, V. Balic, T. Peyronel, M. Hafezi, A. S. Zibrov, V. Vuletic, and M. D. Lukin, "Efficient all-optical switching using slow light within a hollow fiber," Phys. Rev. Lett. **102**, 203902 (2009).
17. A. D. Slepkov, A. R. Bhagwat, V. Venkataraman, P. Londero, and A. L. Gaeta, "Spectroscopy of Rb atoms in hollow-core fibers," Phys. Rev. A **81**, 053825 (2010).
18. F. L. Kien, and K. Hakuta, "Slowing down of a guided light field along a nanofiber in a cold atomic gas," Phys. Rev. A. **79**, 013818 (2009).
19. V. R. Almeida, Q. Xu, C. A. Barrios, R. R. Panepucci, and M. Lipson, "Guiding and confining light in void nanostructure," Opt. Lett. **29**, 1209-1211 (2004).
20. Q. Xu, V. R. Almeida, R. Panepucci, and M. Lipson, "Experimental demonstration of guiding and confining light in nanometer-size low-refractive-index material," Opt. Lett. **29**, 1626-1628 (2004).
21. M. Galli, D. Gerace, A. Politi, M. Liscidini, M. Patrini, L. C. Andreani, A. Canino, M. Miritello, R. L. Savio, A. Irrera, and F. Priolo, "Direct evidence of light confinement and emission enhancement in active silicon-on-insulator slot waveguides," Appl. Phys. Lett. **89**, 241114 (2006).
22. K. Foubert, L. Lalouat, B. Cluzel, E. Picard, D. Peyrade, F. de Fornel, and E. Hadji, "An air-slotted nanoresonator relying on coupled high Q small V Fabry-Perot nanocavities," Appl. Phys. Lett. **94**, 251111 (2009).
23. T. Yamamoto, M. Notomi, H. Taniyama, E. Kuramochi, Y. Yoshikawa, Y. Torii, and T. Kuga, "Design of a high-Q air-slot cavity based on a width-modulated line-defect in a photonic crystal slab," Opt. Express **16**, 13809-13817 (2008).
24. Y. Li, J. Zheng, J. Gao, J. Shu, M. S. Aras, and C. W. Wong, "Design of dispersive optomechanical coupling and cooling in ultrahigh-Q/V slot-type photonic crystal cavities," Opt. Express **18**, 23844-23856 (2010).
25. M. P. Hiscocks, C. Su, B. C. Gibson, A. D. Greentree, L. C. L. Hollenberg, and F. Ladouceur, "Slot-waveguide cavities for optical quantum information applications," Opt. Express **17**, 7295-7303 (2009).
26. H. Ryu, J. Kim, Y. M. Jhon, S. Lee, and N. Park, "Effect of index contrasts in the wide spectral-range control of slot waveguide dispersion," Opt. Express **20**, 13189-13194 (2012)
27. C. Koos, L. Jacome, C. Poulton, J. Leuthold, and W. Freude, "Nonlinear silicon-on-insulator waveguides for all-optical signal processing," Opt. Express **15**, 5976-5990 (2007).
28. P. Muellner, M. Wellenzohn, and R. Hainberger, "Nonlinearity of optimized silicon photonic slot waveguides," Opt. Express **17**, 9282-9287 (2009).
29. Q. Quan, I. Bulu, and M. Lončar, "Broadband waveguide QED system on a chip," Phys. Rev. A. **80**, 011810(R) (2009).
30. L. Zhang, Y. Yue, Y. X. Li, J. Wang, R. G. Beausoleil, and A. E. Willner, "Flat and low dispersion in highly nonlinear slot waveguides," Opt. Express **18**, 13187-13193 (2010).
31. Y. Yue, L. Zhang, J. Wang, R. G. Beausoleil, and A. E. Willner, "Highly efficient nonlinearity reduction in silicon-on-insulator waveguides using vertical slots," Opt. Express **18**, 22061-22066 (2010).
32. R. Guo, B. Wang, X. Wang, L. Wang, L. Jiang, and Z. Zhou, "Optical amplification in Er/Yb silicate slot waveguide," Opt. Lett. **37**, 1427-1429 (2012).
33. H. Lee, Y. Rostovtsev, C. J. Bednar, and A. Javan, "From laser-induced line narrowing to electro- magnetically induced transparency: closed system analysis," Appl. Phys. B **76**, 33 (2003).
34. L. Li, and G. Huang, "Linear and nonlinear light propagations in a Doppler-broadened medium via electromagnetically induced transparency," Phys. Rev. A **82**, 023809 (2010).

1. Introduction

Over the past two decades, quantum interference phenomena has attracted much attention due to their fundamental interest and promising applications for optical and quantum information processing. One of such phenomena is electromagnetically induced transparency (EIT), which can be used to substantially enhance the efficiency of nonlinear optical processes in addition to a large suppression of optical absorption [1]. Another noticeable effect of EIT is drastic reduction of group velocity of optical pulses, which has important applications such as slow

#180953 - $15.00 USD Received 30 Nov 2012; revised 13 Jan 2013; accepted 15 Jan 2013; published 22 Feb 2013

light [2, 3], quantum memory [4–6], quantum phase gates [7, 8], and slow light solitons [9, 10].

However, up to now most works on EIT and optical pulse propagations have been performed with atomic gases in bulk samples [1]. Since optical pulses in such systems are unguided plane waves, interaction strength between optical pulses and quantum emitters is limited and thus EIT effect is weak. It is desirable to use optical waveguides where optical fields are guided and optical energy is concentrated in small spatial regions. Such structures can be used to not only for enhancing EIT effect, but also for raising the efficiency of nonlinear optical processes based on gases phase media such as atoms or molecules. In recent years, there have been several works on EIT and related studies in waveguide structures where atomic or molecular gases are filled in low-index regions, including hollow-core photonic crystal fibers [11–17], nanofibers [18], and so on.

Guiding light in low-refractive-index materials (e.g air) is thought to be prohibited in conventional waveguides based on total internal reflection. Usually, multiple dielectric layers [11] or hollow-core photonic crystal fibers [12–17] based on external reflections are adopted. However, in order to have high reflections, such structures have relatively large dimensions and are wavelength sensitive. In 2004, Almeida *et al*. [19] proposed a novel structure called slot waveguide, which consists of a nanometer-size slot filled with a low-index material and embedded in high-index materials. In such structure, light is also guided by total internal reflection but it can be tightly confined and hence largely enhanced in the slot region [20, 21]. Recently, There have been a large amount of research activities on guiding and confining light by using slot waveguides [22–32].

In this article, we propose a scheme to enhance quantum interference effect by using a Λ-type three-level atomic gas filled in a slot waveguide, in which electric field is strongly confined inside the slot of the waveguide due to the discontinuity of dielectric constant. We find that the EIT effect can be greatly enhanced due to reduction of optical-field mode volume contributed by waveguide geometry. Comparing with atomic gases in free space, the EIT transparency window in the slot-waveguide system is much wider and deeper, and Kerr nonlinearity of probe laser field is much stronger. We also demonstrate that using the slot waveguide ultraslow optical solitons can be produced more efficiently and their generation power is extremely low.

The rest of the article is organized as follows. Sec. 2 describes our theoretical model. Sec. 3 studies the linear propagation of probe field and analyzes its EIT characters. Sec. 4 discusses nonlinear pulse propagation in the slot waveguide system. Finally, the last section summarizes the main results obtained in this work.

2. Model

The slot waveguide we adopt is similar to that suggested in Ref. [19], which is shown in the left part of Fig. 1. It consists of a very thin slot (with width $2a$ in z-direction) of low-index material (with index n_S) embedded between two thick rectangular regions (with width $b-a$ on both sides) of high-index material (with index n_H), both surrounded by a low-index cladding (with index n_C). Sizes in the x- and y-directions of each rectangular region are much larger than a and b. It has been shown [19] that such slot waveguide has the ability for concentrating electromagnetic (EM) field of transverse magnetic (TM) modes basically within the slot region, and hence is very attractive for enhancing radiation-matter interaction. The expressions of guided TM eigenmodes of eigenfrequencies $\omega_m(k_\parallel)$ are given in Appendix A. Here $k_\parallel = (k_x^2 + k_y^2)^{1/2}$ with k_x and k_y being respectively the wavenumbers in x- and y-directions. The physical reason of the confinement and enhancement of TM modes is quite simple. For interfaces with high-index contrast, Maxwell's equations require a continuity of normal component of electric displacement vector, which gives that electric field in the slot region is $(n_H/n_S)^2$ times higher than that in the high-index region.

#180953 - $15.00 USD Received 30 Nov 2012; revised 13 Jan 2013; accepted 15 Jan 2013; published 22 Feb 2013

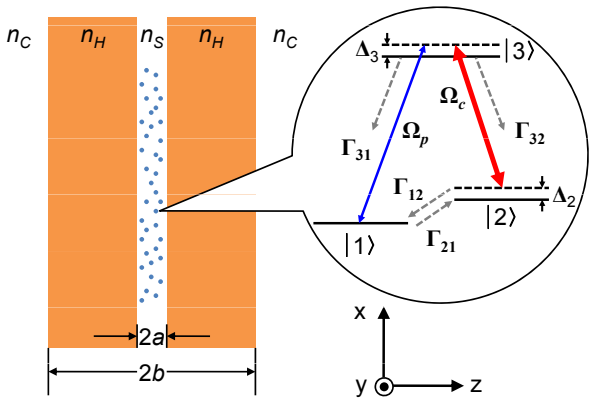

Fig. 1. Left: Schematic of slot waveguide structure. The slot width (index n_S) is $2a$, the width of the high-index silicon slabs (index n_H) is $2b-2a$. The index of the cladding material is n_C. Right: Level diagram of the three-level atomic system. Ground state $|1\rangle$ couples to the exited $|2\rangle$ and $|3\rangle$ with the control field Ω_c and the probe field Ω_p. Δ_2 and Δ_3 are the detunings of control and probe fields, respectively. Γ_{31} (Γ_{32}) is the spontaneous emission decay rate from $|3\rangle$ to $|1\rangle$ ($|2\rangle$). Γ_{12} and Γ_{21} are incoherent population exchange rates. Below the level diagram is the coordinate system chosen for theoretical calculations. The slot region is $|z|\leq a$, and the slabs are in the region $a<|z|<b$.

Since k_x, k_y can take any continuous values, and m takes non-zero integers (i.e. $m=1,2,3,\cdots$), the guided TM eigenmodes propagate in the xy-plane but is confined in the slot region of the waveguide. For simplicity, we study the lowest-order (i.e. $m=1$) TM guided mode, and assume $k_x=0$, $k_y=k$ without loss of generality. Then from the Appendix A we have $\mathbf{k}_{\|}=(0,k,0)$, $\hat{\mathbf{k}}_{\|}=\mathbf{e}_y$, $k_{\|}=k$, and

$$\mathbf{E}^{\mathrm{TM}}(\mathbf{r},t)=\sum_k\sqrt{\frac{\hbar\omega_1(k)}{2\varepsilon_0 V_1}}\mathbf{u}_{1,k}(z)a_1(k)e^{i[ky-\omega_1(k)t]}+\text{c.c.}, \tag{1a}$$

$$\mathbf{u}_{1,k}(z)=\frac{c}{2\sqrt{N_1}\omega_1(k)n^2(z)}\left[kH_{1,k}(z)\mathbf{e}_z+i\frac{dH_{1,k}(z)}{dz}\mathbf{e}_y\right]. \tag{1b}$$

Here $\omega_1(k)=(\kappa_{H1}^2+k^2)^{1/2}c/n_H=(k^2-\gamma_{S1}^2)^{1/2}c/n_S$, V_1 is the mode volume, $\mathbf{e}_y$ ($\mathbf{e}_z$) is the unit vector along the y (z) direction, $\mathbf{u}_{1,k}(z)$ is the mode function satisfying $\int_{-\infty}^{\infty}dz|\mathbf{u}_{1,k}(z)|^2=V_1$, $\varepsilon(z)\equiv n^2(z)$ is dielectric function with $n(z)=n_S$ ($|z|<a$), n_H ($a<|z|<b$), and n_C ($|z|>b$) (see Fig. 1). The concrete expressions of V_1 and N_1 (normalized constant) can be found in the Appendix A (i.e. Eq. (27)) for $m=1$.

For convenience, we take k as a function of ω_1. Replacing ω_1 by ω, the electric-field expression of the lowest-order TM guided mode reads $\mathbf{E}^{\mathrm{TM}}(\mathbf{r},t)=\sum_\omega\mathscr{E}_\omega(\frac{W_1}{V_1})^{\frac{1}{2}}\mathbf{u}_{1,\omega}(z)\,e^{i[k(\omega)y-\omega t)]}+$ c.c., with $\mathbf{u}_{1,\omega}(z)\equiv\{c/[\sqrt{N_1}\omega n^2(z)]\}\{[kH_{1,\omega}(z)\mathbf{e}_z+i[dH_{1,\omega}(z)/dz]\mathbf{e}_y\}$. Here $k(\omega)=[n_H^2\omega^2/c^2-\kappa_{H1}^2]^{1/2}=[\gamma_{S1}^2+n_S^2\omega^2/c^2]^{1/2}$ and $\mathscr{E}_\omega=\sqrt{\frac{\hbar\omega}{2\varepsilon_0 W_1}}a_1(\omega)$, with W_1 being the mode volume without the slot (its expression is given in the Appendix B (i.e. Eq. (30)) for $m=1$), which is taken to be a reference mode volume for the discussions in the following.

Our aim is to investigate the resonant interaction between the TM-mode of EM field and quantum emitters that are embedded in the slot of the waveguide. For simplicity, we assume the media in the slot and the cladding regions are air (i.e. $n_S=n_C=1$), and the quantum emitters

#180953 - $15.00 USD Received 30 Nov 2012; revised 13 Jan 2013; accepted 15 Jan 2013; published 22 Feb 2013

are gaseous atoms with a Λ-type three-level configuration (see the right part of Fig. 1), which is filled in the slot region. Atomic energy levels are two ground states $|1\rangle$ and $|2\rangle$ and one exited state $|3\rangle$, which couple with a weak, pulsed probe field with center angular frequency $\omega_p = k_p/c$ and half Rabi frequency Ω_p (i.e. $|1\rangle \to |3\rangle$ transition) and a strong, continuous-wave control field of center angular frequency $\omega_c = k_c/c$ and half Rabi frequency Ω_p (i.e. $|2\rangle \to |3\rangle$ transition). Γ_{31} (Γ_{32}) is the spontaneous emission decay rate from $|3\rangle$ to $|1\rangle$ ($|2\rangle$). Γ_{21} (Γ_{12}) is the incoherent population exchange rate from $|1\rangle$ to $|2\rangle$ ($|2\rangle$ to $|1\rangle$), introduced to reflect the transient relaxation process of the atoms entering and leaving interaction region. We assume that both the probe and control fields belong to the lowest-order TM guided mode given in Eq. (1), which has the form

$$\mathbf{E}^{\mathrm{TM}}(\mathbf{r},t) = \sum_{l=p,c} \mathscr{E}_l \left(\frac{W_1}{V_1}\right)^{\frac{1}{2}} \mathbf{u}_{1,l}(z) \exp\{i[k(\omega_l)y - \omega_l t]\} + \text{c.c.}. \tag{2}$$

The Hamiltonian of the system in interaction picture reads

$$\hat{\mathscr{H}} = -\hbar \sum_j^3 \Delta_j |j\rangle\langle j| - \hbar[\zeta_p^*(z)\Omega_p^*|1\rangle\langle 3| + \zeta_c^*(z)\Omega_c^*|2\rangle\langle 3| + h.c.], \tag{3}$$

where $\Delta_3 \equiv \omega_p - (\omega_3 - \omega_1)$ and $\Delta_2 \equiv \omega_p - \omega_c - (\omega_2 - \omega_1)$ are respectively the one- and two-photon detunings, $\zeta_p(z) \equiv (\frac{W_1}{V_1})^{\frac{1}{2}} \mathbf{e}_{31} \cdot \mathbf{u}_{1,p}(z)$ and $\zeta_c(z) \equiv (\frac{W_1}{V_1})^{\frac{1}{2}} \mathbf{e}_{32} \cdot \mathbf{u}_{1,c}(z)$ are respectively the mode functions of the probe and control fields, $\Omega_p \equiv p_{31}\mathscr{E}_p/\hbar$ and $\Omega_c \equiv p_{32}\mathscr{E}_c/\hbar$ are respectively their corresponding half Rabi frequencies, with $\mathbf{e}_{jl}$ the unit vector of the electric dipole matrix element $\mathbf{p}_{jl}$, i.e. $\mathbf{p}_{jl} = \mathbf{e}_{jl} p_{jl}$.

Taking Doppler effect into account, the equation of motion of σ_{jl}, i.e. the density matrix elements in the interaction picture, are given by

$$i\frac{\partial}{\partial t}\sigma_{11} + i\Gamma_{21}\sigma_{11} - i\Gamma_{12}\sigma_{22} - i\Gamma_{13}\sigma_{33} + \zeta_p^*(z)\Omega_p^*\sigma_{31} - \zeta_p(z)\Omega_p\sigma_{31}^* = 0, \tag{4a}$$

$$i\frac{\partial}{\partial t}\sigma_{22} - i\Gamma_{21}\sigma_{11} + i\Gamma_{12}\sigma_{22} - i\Gamma_{23}\sigma_{33} + \zeta_c^*(z)\Omega_c^*\sigma_{32} - \zeta_c(z)\Omega_c\sigma_{32}^* = 0, \tag{4b}$$

$$\begin{aligned} i\frac{\partial}{\partial t}\sigma_{33} + i(\Gamma_{13}+\Gamma_{23})\sigma_{33} - \zeta_p^*(z)\Omega_p^*\sigma_{31} + \zeta_p(z)\Omega_p\sigma_{31}^* \\ -\zeta_c^*(z)\Omega_c^*\sigma_{32} + \zeta_c(z)\Omega_c\sigma_{32}^* = 0, \end{aligned} \tag{4c}$$

$$\left(i\frac{\partial}{\partial t} + d_{21}\right)\sigma_{21} - \zeta_p(z)\Omega_p\sigma_{32}^* + \zeta_c^*(z)\Omega_c^*\sigma_{31} = 0, \tag{4d}$$

$$\left(i\frac{\partial}{\partial t} + d_{31}\right)\sigma_{31} - \zeta_p(z)\Omega_p(\sigma_{33} - \sigma_{11}) + \zeta_c(z)\Omega_c\sigma_{21} = 0, \tag{4e}$$

$$\left(i\frac{\partial}{\partial t} + d_{32}\right)\sigma_{32} - \zeta_c(z)\Omega_c(\sigma_{33} - \sigma_{22}) + \zeta_p(z)\Omega_p\sigma_{21}^* = 0, \tag{4f}$$

where $d_{21} = -(k_p - k_c)v + \Delta_2 + i\gamma_{21}$, $d_{31} = -k_p v + \Delta_3 + i\gamma_{31}$ and $d_{32} = -k_c v + (\Delta_3 - \Delta_2) + i\gamma_{32}$ (with v the atom velocity), $\Gamma_j = \sum_{j>i}\Gamma_{ij}$ and $\gamma_{ij} = (\Gamma_i + \Gamma_j)/2 + \gamma_{ij}^{\mathrm{col}}$ are population and coherence decay rates, respectively. Here Γ_{ij} represents the spontaneous emission decay rate from state $|j\rangle$ to state $|i\rangle$, $\gamma_{ij}^{\mathrm{col}}$ are dephasing rates, and Γ_{21} is the incoherent population exchange from state $|1\rangle$ to state $|2\rangle$. Note that the atom-photon interactions in waveguide geometries may introduce some undesirable effects, such as the atomic collisions with waveguide walls and the adhesion to the walls [17]. We assume these interfacial effects can be weakened by using similar experimental techniques as did in Refs. [13, 16, 17], like coating the inner walls with

#180953 - $15.00 USD Received 30 Nov 2012; revised 13 Jan 2013; accepted 15 Jan 2013; published 22 Feb 2013

some materials (i.e. paraffin) or using light-induced atomic desorption. Note that the controlling field Rabi frequency Ω_c in our system is strong enough, so that the change of the decay rate due to the confinement of atoms plays no significant role.

The electric polarization intensity of the system reads

$$\mathbf{P} = \mathscr{N}_a \int_{-\infty}^{\infty} dv f(v)[\mathbf{p}_{13}\sigma_{31}e^{i(k_p y-\omega_p t)} + \mathbf{p}_{23}\sigma_{32}e^{i(k_c y-\omega_c t)} + \text{c.c.}], \tag{5}$$

where $\mathscr{N}_a$ is atomic concentration, $f(v) = 1/(\sqrt{\pi}v_T)\exp[-(v/v_T)^2]$ is Maxwell velocity distribution, $v_T = \sqrt{2k_BT/M}$ is the most probable speed at temperature T, with M the atomic mass and k_B the Boltzmann constant. Because the integration over the Maxwell distribution is not easy to analyze, as did in Refs. [33, 34] we replace it by the modified Lorentzian velocity distribution $f(v) = v_T/[\sqrt{\pi}(v^2+v_T^2)]$.

The motion of the electric field is controlled by Maxwell equation, which under the slowly varying envelope approximation reduces to

$$i\left(\frac{\partial}{\partial y} + \frac{1}{c}\frac{\langle n^2(z)\rangle}{n_{\text{eff}}}\frac{\partial}{\partial t}\right)\Omega_p + \frac{c}{2\omega_p n_{\text{eff}}}\frac{\partial^2\Omega_p}{\partial x^2} + \kappa_{13}\int_{-\infty}^{\infty} dv f(v)\langle\sigma_{31}(v,z)\rangle = 0, \tag{6}$$

where $\kappa_{13} = N\omega_p|\mathbf{p}_{13}|^2/(2\varepsilon_0\hbar c n_{\text{eff}})$ and $n_{\text{eff}} = ck(\omega_p)/\omega_p$ is the effective refraction index. The quantity $\langle Q(z)\rangle \equiv \int_{-\infty}^{\infty} dz\zeta^*(z)Q(z)/\int_{-\infty}^{\infty} dz|\zeta(z)|^2$ for any function of $Q(z)$.

3. EIT characters

3.1. Base state

When the probe field is absent (i.e. $\Omega_p = 0$), the Maxwell-Bloch (MB) Eqs. (4), (6) have the steady-state solution

$$\sigma_{11}^{(0)} = \frac{\Gamma_{12}(\Gamma_{13}+\Gamma_{23})X_1 + (\Gamma_{12}+\Gamma_{13})|\zeta(z)\Omega_c|^2}{X_2}, \tag{7a}$$

$$\sigma_{22}^{(0)} = \frac{\Gamma_{21}(\Gamma_{13}+\Gamma_{23})X_1 + \Gamma_{21}|\zeta(z)\Omega_c|^2}{X_2}, \tag{7b}$$

$$\sigma_{33}^{(0)} = \frac{\Gamma_{21}|\zeta(z)\Omega_c|^2}{X_2}, \tag{7c}$$

$$\sigma_{32}^{(0)} = -\frac{\zeta(z)\Omega_c}{d_{32}}\frac{\Gamma_{21}(\Gamma_{13}+\Gamma_{23})X_1}{X_2}, \tag{7d}$$

and $\sigma_{21}^{(0)} = \sigma_{31}^{(0)} = 0$, where $X_1 = \{[k_c v - (\Delta_3-\Delta_2)]^2 + \gamma_{32}^2\}/2\gamma_{32}$ and $X_2 = (\Gamma_{12}+\Gamma_{21})(\Gamma_{13}+\Gamma_{23})X_1 + (\Gamma_{12}+2\Gamma_{21}+\Gamma_{13})|\zeta(z)\Omega_c|^2$. Note that we have taken $\zeta_c(z) \approx \zeta_p(z) \equiv \zeta(z)$ because $\omega_p \approx \omega_c$.

From (7) we see that, due to the incoherent population exchange, there are population occupation in all three levels. However, the population in states $|2\rangle$ and $|3\rangle$ are small because generally Γ_{21} and Γ_{12} are small. When $\Gamma_{21} = \Gamma_{12} = 0$, one has $\sigma_{11} = 1$ and $\sigma_{jl} = 0$ $(j,l \neq 1)$.

3.2. EIT characters

We now study the solution of linear excitations of the system, which can be done by linearizing the MB Eqs. (4) and (6) around the base state (7). Taking $\sigma_{jj} = \sigma_{jj}^{(0)}(j = 1,2,3)$, $\sigma_{32} = \sigma_{32}^{(0)}$, and assuming Ω_p and σ_{j1} are small quantities proportional to $\exp[i(K(\omega)y - \omega t)]$, we obtain

#180953 - $15.00 USD Received 30 Nov 2012; revised 13 Jan 2013; accepted 15 Jan 2013; published 22 Feb 2013

the linear dispersion relation

$$K(\omega)=\frac{1}{\int_{-\infty}^{\infty}dz|\zeta(z)|^2}\int_{-\infty}^{\infty}dz|\zeta(z)|^2\Big\{\frac{\omega}{c}\frac{n^2(z)}{n_{eff}} + \kappa_{13}\int_{-\infty}^{\infty}dv f(v)\frac{\zeta(z)\Omega_c\sigma_{32}^{*(0)}+(\omega+d_{21})(2\sigma_{11}^{(0)}+\sigma_{22}^{(0)}-1)}{|\zeta(z)\Omega_c|^2-(\omega+d_{21})(\omega+d_{31})}\Big\}. \tag{8}$$

Different from the case in free space [34], here we must calculate two-fold integration. The first one is the second term in the brace, which is a statistical average on atomic velocity v. Such integration can be calculated by the use of residue theorem [34]. Taking $k_p v$ as a complex number, we find two poles in the lower half complex plane, given by $k_p v=-ik_p v_T$ and $k_p v=-i\{\gamma_{32}^2+2\gamma_{32}(\Gamma_{12}+2\Gamma_{21}+\Gamma_{13})|\zeta(z)\Omega_c|^2/[(\Gamma_{12}+\Gamma_{21})\Gamma_3]\}^{1/2}\equiv-i\eta$. For calculating the integration, we take a contour consisting of the lower half complex plane and real axis. The use of residue theorem gives

$$K(\omega)=\int_{-\infty}^{\infty}dz|\zeta(z)|^2\left(\frac{\omega}{c}\frac{n^2(z)}{n_{\rm eff}}+\mathscr{K}_1(z)+\mathscr{K}_2(z)\right)\Big/\int_{-\infty}^{\infty}dz|\zeta(z)|^2, \tag{9}$$

where $\mathscr{K}_1$ is the contribution from the first pole point $k_p v=-ik_p v_T$:

$$\begin{aligned}\mathscr{K}_1(z)=&\sqrt{\pi}\kappa_{13}\Big\{|\zeta(z)\Omega_c|^2\Gamma_{21}\Gamma_3(-i\Delta\omega_D-i\gamma_{32})\\&+(\omega+i\gamma_{21})[\Gamma_{12}\Gamma_3(-\Delta\omega_D^2+\gamma_{32}^2)+2\gamma_{32}(\Gamma_{12}-\Gamma_{21}+\Gamma_{13})|\zeta(z)\Omega_c|^2]\Big\}\\&\Big/\Big\{(-\Delta\omega_D^2+\eta^2)(\Gamma_{12}+\Gamma_{21})\Gamma_3[|\zeta(z)\Omega_c|^2-(\omega+i\gamma_{21})(\omega+i\Delta\omega_D+i\gamma_{31})]\Big\},\end{aligned} \tag{10}$$

and $\mathscr{K}_2$ is the contribution from the second pole point $k_p v=-i\eta$

$$\begin{aligned}\mathscr{K}_2(z)=&\sqrt{\pi}\kappa_{13}\Delta\omega_D\Big\{|\zeta(z)\Omega_c|^2\Gamma_{21}\Gamma_3(-i\eta-i\gamma_{32})\\&+(\omega+i\gamma_{21})[\Gamma_{12}\Gamma_3(-\eta^2+\gamma_{32}^2)+2\gamma_{32}(\Gamma_{12}-\Gamma_{21}+\Gamma_{13})|\zeta(z)\Omega_c|^2]\Big\}\\&\Big/\Big\{\eta(\Delta\omega_D^2-\eta^2)(\Gamma_{12}+\Gamma_{21})\Gamma_3[|\zeta(z)\Omega_c|^2-(\omega+i\gamma_{21})(\omega+i\eta+i\gamma_{31})]\Big\}.\end{aligned} \tag{11}$$

The integration on z in Eq. (9) is a spatial average due to the EM field confinement by the waveguide geometry, which must be done numerically.

The expression of the imaginary part of $K(\omega)$ at $\omega=0$, i.e. $\mathrm{Im}(K_0)$, is given by

$$\begin{aligned}\mathrm{Im}(K_0)=&\frac{1}{\int_{-\infty}^{\infty}dz|\zeta(z)|^2}\int_{-\infty}^{\infty}dz|\zeta(z)|^2\int_{-\infty}^{\infty}dv f(v)\frac{\kappa_{13}\gamma_{21}}{|\zeta(z)\Omega_c|^2+\gamma_{21}\gamma_{31}}\\&\times\Big(1-\frac{\Gamma_{21}\Gamma_3X_1+3\Gamma_{21}|\zeta(z)\Omega_c|^2}{(\Gamma_{21}+\Gamma_{12})\Gamma_3X_1+(2\Gamma_{21}+\Gamma_{12}+\Gamma_{13})|\zeta(z)\Omega_c|^2}\Big).\end{aligned} \tag{12}$$

From Eq. (9) to Eq. (12) we obtain the following conclusions:

(1). The linear dispersion relation $K(\omega)$ depends strongly on the slot width $2a$ due to the factor $(W_1/V_1)^{1/2}$ appeared in the mode function $\zeta(z)$. Shown in Fig. 2(a) is the probe-field absorption spectrum $\mathrm{Im}(K)$ as a function of ω for different slot width. The red solid, black dashed and blue dashed-dotted lines are for $2a=50,30$ and 10 nm, respectively. We see that: (i) For three different slot widths, an EIT transparency window (i.e. the dip near $\omega=0$) is opened. (ii) The width of the EIT transparency window becomes larger as the slot width $2a$ decreases,

#180953 - $15.00 USD Received 30 Nov 2012; revised 13 Jan 2013; accepted 15 Jan 2013; published 22 Feb 2013

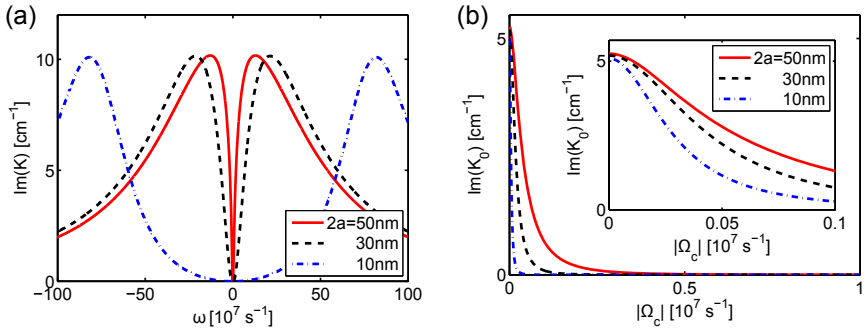

Fig. 2. (a): Im(K) as a function of frequency ω for different slot width $2a$. The red solid, black dashed, and blue dashed-dotted lines are for the slot width $2a = 50, 30$ and 10 nm, respectively. (b): Im(K_0) as a function of $|\Omega_c|$ for different slot width $2a$. The red solid, black dashed, and blue dashed-dotted lines are for the slot width $2a = 50, 30, 10$ nm, respectively.

which means that quantum interference effect is enhanced when the slot width decreases. The physical reason of the enhancement of EIT effect is due to the reduction of EM-field mode volume, which results in $(W_1/V_1)^{1/2} \gg 1$ and hence the giant enhancement of the interaction between light and atoms.

(2). The minimum of the absorption, i.e. Im(K_0), depends not only on Ω_c but also on the slot width. Fig. 2(b) shows the profile of Im(K_0) as a function of Rabi frequency $|\Omega_c|$ for different slot width $2a$, where the red solid, black dashed and blue dashed-dotted lines are for $2a = 50, 30$ and 10 nm, respectively. One sees that: (i) For a given Ω_c, Im(K_0) for smaller slot width is obviously much smaller than that for larger slot width. As the slot width decreases, the EIT transparency window can be not only widened but also deepened dramatically. (ii) The EIT transparency window with a smaller slot width can be obtained with a much smaller Ω_c than that with a larger slot width, which means that the confinement provided by the waveguide geometry can be used to get an EIT more easily than that without the confinement. Note that when plotting Fig. 2 we have used a practical example with the D_1 line transition of ^{87}Rb atoms, by selecting$|5S_{1/2}, F = 1\rangle$, $|5S_{1/2}, F = 2\rangle$, and $|5P_{1/2}, F = 1\rangle$ as the atomic states $|1\rangle$, $|2\rangle$, and $|3\rangle$, respectively. The system parameters used are $\kappa_{13} = 1.0 \times 10^9$ cm^{-1}s^{-1}, $\Omega_c = 1.0 \times 10^8$ s^{-1}, $\Gamma_{31} = \Gamma_{32} = 1.0 \times 10^7$ s^{-1}, and $\Gamma_{21} = 10^{-4}\Gamma_{31}$.

(3). The incoherent population exchange (i.e. nonzero Γ_{21}) plays no significant role on the probe-field absorption when Ω_c is very large. However, it has non-negligible influence when Ω_c is not too large, reflected in the second term (i.e. the term related to Γ_{21}) in the bracket of Eq. (12) which contributes a obvious reduction to the absorption of the probe field. In fact, by the incoherent population exchange the atoms undergo an active Raman gain process from $|2\rangle \to |3\rangle \to |1\rangle$. Shown in Fig. 3(a) is Im(K) as function of frequency ω for $\Omega_c = 1.0 \times 10^6$ s^{-1} with $\Gamma_{21} = 0$ (red solid line), $\Gamma_{21} = 0.5\Gamma_{12}$ (black dashed line) and $\Gamma_{21} = \Gamma_{12}$ (blue dashed-dotted line), respectively. We see that the absorption for $\Gamma_{21} = \Gamma_{12}$ is much smaller than that for $\Gamma_{21} = 0$. So a incoherent population exchange can be used to widen and deepen the EIT transparency window. Fig. 3(b) shows the profile of Im(K_0) as a function of $|\Omega_c|$ with $\Gamma_{21} = 0$ (red solid line), $\Gamma_{21} = 0.5\Gamma_{12}$ (black dashed line) and $\Gamma_{21} = \Gamma_{12}$ (blue dashed-dotted line), respectively. We see that for large $|\Omega_c|$, there is no obvious difference in Im(K_0) for different Γ_{21}; but for small $|\Omega_c|$ the effect caused by Γ_{21} can be observed clearly.

#180953 - $15.00 USD Received 30 Nov 2012; revised 13 Jan 2013; accepted 15 Jan 2013; published 22 Feb 2013

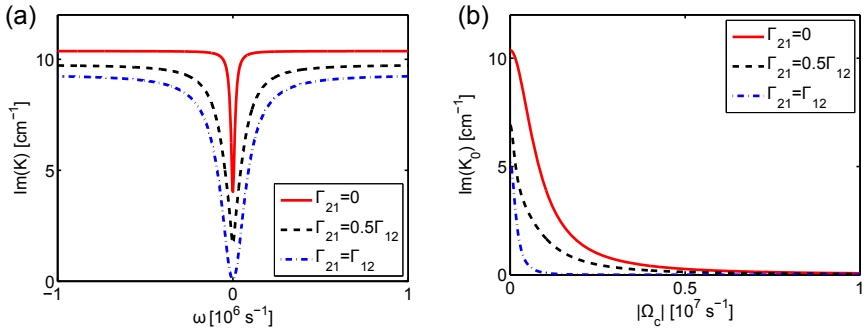

Fig. 3. (a): Im(K) as a function of ω. (b): Im(K_0) as a function of $|\Omega_c|$ with $\Gamma_{21}=0$ (red solid line), $\Gamma_{21}=0.5\Gamma_{12}$ (black dashed line) and $\Gamma_{21}=\Gamma_{12}$ (blue dashed-dotted line), respectively.

4. Kerr nonlinearity and ultraslow optical solitons

4.1. Kerr nonlinearity of the system

From the MB Eqs. (4) and (6), we obtain the probe field susceptibility

$$\chi_p=\int_{-\infty}^{\infty}dv f(v)\frac{\mathcal{N}_a|\mathbf{p_{13}}|^2}{\varepsilon_0\hbar}\frac{\langle\sigma_{31}(v,z)\rangle}{\Omega_p}\approx\chi_p^{(1)}+\chi_{pp}^{(3)}|\mathscr{E}_p|^2, \tag{13}$$

where $\mathscr{E}_p=\hbar\Omega_p/p_{31}$, $\chi_p^{(1)}$ and $\chi_{pp}^{(3)}$ are respectively first-order (linear) and third-order (Kerr) susceptibilities, with the expressions given by

$$\begin{aligned}\chi_p^{(1)} &= \frac{\mathcal{N}_a|\mathbf{p_{13}}|^2}{\varepsilon_0\hbar}\int_{-\infty}^{\infty}dz|\zeta(z)|^2\int_{-\infty}^{\infty}dv f(v)\\ &\quad\times\frac{d_{21}d_{32}^*(\sigma_{33}^{(0)}-\sigma_{11}^{(0)})-|\zeta(z)\Omega_c|^2(\sigma_{33}^{(0)}-\sigma_{22}^{(0)})}{d_{32}^*(d_{21}d_{31}-|\zeta(z)\Omega_c|^2)}\Big/\int_{-\infty}^{\infty}dz|\zeta(z)|^2, \qquad (14a)\\ \chi_{pp}^{(3)} &= \frac{\mathcal{N}_a|\mathbf{p_{13}}|^4}{\varepsilon_0\hbar^3}\frac{1}{\int_{-\infty}^{\infty}dz|\zeta(z)|^2}\int_{-\infty}^{\infty}dz|\zeta(z)|^2\int_{-\infty}^{\infty}dv f(v)\\ &\quad\times|\zeta(z)|^2\Big[id_{32}\zeta(z)\Omega_cZ_1Z_4-(2d_{21}|d_{32}|^2-d_{32}|\zeta(z)\Omega_c|^2)Z_2\\ &\quad-(d_{21}|d_{32}|^2-2d_{32}|\zeta(z)\Omega_c|^2)Z_3\Big]\Big/\Big[iZ_1|d_{32}|^2(|\zeta(z)\Omega_c|^2-d_{21}d_{31})\Big], \qquad (14b)\end{aligned}$$

where $Z_1=(\Gamma_{12}+\Gamma_{21})(\Gamma_{13}+\Gamma_{23})|d_{32}|^2+2\gamma_{32}(\Gamma_{12}+2\Gamma_{21}+\Gamma_{13})|\zeta(z)\Omega_c|^2$, $Z_2=[(\Gamma_{12}+\Gamma_{23})|d_{32}|^2+4\gamma_{32}|\zeta(z)\Omega_c|^2](Z_5-\text{c.c.})+(\Gamma_{12}-\Gamma_{13})[(d_{32}^*\zeta^*(z)\Omega_c^*Z_4^*)-\text{c.c.}]$, $Z_3=(\Gamma_{21}+\Gamma_{13})[(d_{32}^*\zeta^*(z)\Omega_c^*Z_4^*)-\text{c.c.}]-[(-\Gamma_{21}+\Gamma_{23})|d_{32}|^2+2\gamma_{32}|\zeta(z)\Omega_c|^2](Z_5-\text{c.c.})$, $Z_4=[-d_{31}\sigma_{32}^{*(0)}-\zeta^*(z)\Omega_c^*(\sigma_{11}^{(0)}-\sigma_{33}^{(0)})]/(|\zeta(z)\Omega_c|^2-d_{21}d_{31})$ and $Z_5=[\zeta(z)\Omega_c\sigma_{32}^{(0)}+d_{21}^*(\sigma_{11}^{(0)}-\sigma_{33}^{(0)})]/(|\zeta(z)\Omega_c|^2-d_{21}^*d_{31}^*)$.

The Kerr effect can be enhanced due to the confinement effect induced by the waveguide geometry. When the slot width $2a$ decreases, the confinement of the light field increases because the factor (W_1/V_1) in the expression $|\zeta(z)|^2$ increases. Shown in Fig. 4 is the real part of the third-order susceptibility, i.e. $\text{Re}(\chi_{pp}^{(3)})$, as a function of detunning Δ_3 for different slot width $2a$, where the red solid, black dashed and blue dashed-dotted lines are for $2a=50,25$ and 5 nm, respectively. Parameters are the same as those used in Fig. 2 with a small air ($\varepsilon_S=1$) slot embedded between the silicon ($\varepsilon_H=14$) slabs. We see that the Kerr effect for large confinement

#180953 - $15.00 USD Received 30 Nov 2012; revised 13 Jan 2013; accepted 15 Jan 2013; published 22 Feb 2013

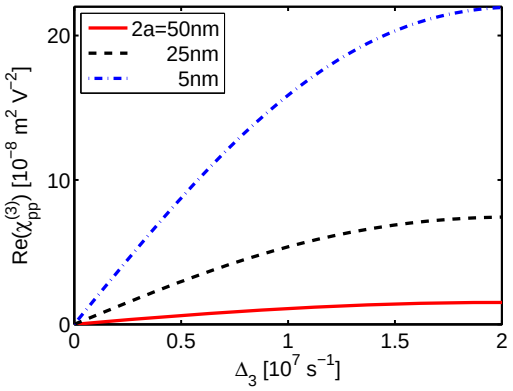

Fig. 4. Third-order susceptibility $\mathrm{Re}(\chi_{pp}^{(3)})$ as a function of detunning Δ_3 for different slot width $2a$. The red solid, black dashed and blue dashed-dotted lines are for $2a = 50, 25$ and 5 nm, respectively.

($2a = 5$ nm) is much larger than that for small confinement ($2a = 50$ nm). Hence the effect of self-phase modulation becomes stronger as the slot size $2a$ goes smaller, which indicates that in the slot waveguide the efficiency of producing ultraslow optical solitons may be higher than that in free space.

4.2. Asymptotic expansion and nonlinear envelope equation

We now turn to study possible optical solitons in the system, which is especially interesting for the present slot waveguide geometry because the light power density in such system is increased and diffraction is suppressed in the confined direction, and thus optical solitons are easy to produce than in free space [9, 10]. Such study is also of practical interest in optical information processing and transmission in quantum hybrid systems when shape-preserving probe pulses with low light power are needed.

To this end, we employ the method of multiple scales to solve the MB equations for nonlinear propagation problems developed in Ref. [10]. Taking the asymptotic expansion $\sigma_{ij} = \sum_{l=0} \varepsilon^{(l)} \sigma_{ij}^{(l)}$, $\Omega_p = \sum_{l=1} \varepsilon^{(l)} \Omega_p^{(l)}$, where $\sigma_{ij}^{(0)}$ is the base state solution given by Eq. (7) and ε is a dimensionless small parameter characterizing the amplitude of the probe field. To obtain a divergence-free expansion, all quantities on the right hand side of the expansion are considered as functions of the multi-scale variables $y_\beta = \varepsilon^\beta y$ ($\beta = 0, 1, 2$) and $t_\beta = \varepsilon^\beta t$ ($\beta = 0, 1$). Substituting the expansion into the MB Eqs. (4) and (6), we obtain a series of equations for $\sigma_{ij}^{(l)}$ and $\Omega_p^{(l)}$, which can be solved order by order.

At the first order ($l = 1$), we obtain the linear solution

$$\Omega_p^{(1)} = F e^{i\theta}, \tag{15a}$$

$$\sigma_{31}^{(1)} = \frac{(\omega + d_{21})(2\sigma_{11}^{(0)} + \sigma_{22}^{(0)} - 1) + \zeta(z)\Omega_c \sigma_{32}^{*(0)}}{|\zeta^2(z)\Omega_c|^2 - (\omega + d_{21})(\omega + d_{31})} \zeta(z) F e^{i\theta}, \tag{15b}$$

$$\sigma_{21}^{(1)} = -\frac{(\omega + d_{31})\sigma_{32}^{*(0)} + \zeta_c^*(z)\Omega_c^*(2\sigma_{11}^{(0)} + \sigma_{22}^{(0)} - 1)}{|\zeta^2(z)\Omega_c|^2 - (\omega + d_{21})(\omega + d_{31})} \zeta(z) F e^{i\theta}, \tag{15c}$$

with other $\sigma_{ij}^{(1)} = 0$. Here $\theta = K(\omega)y_0 - \omega t_0$, with F being a yet to be determined envelope

#180953 - $15.00 USD Received 30 Nov 2012; revised 13 Jan 2013; accepted 15 Jan 2013; published 22 Feb 2013

function depending on the slow variables (t_1, y_1,y_2) and $K(\omega)$ being the linear dispersion relation given by Eq. (8).

At the second order ($l = 2$), the condition of the solution in this order is divergence-free requires $i[\partial F/\partial y_1 + (1/v_g)\partial F/\partial t_1] = 0$, where $v_g = \partial K/\partial\omega$ is the group velocity of the envelope function F. The explicit expressions of the second-order solution are omitted here for saving space.

At the third order ($l = 3$), we obtain the closed equation for F:

$$i\frac{\partial F}{\partial y_2} + \frac{c}{2\omega_p n_{\text{eff}}}\frac{\partial^2 F}{\partial x_1^2} - \frac{K_2}{2}\frac{\partial^2 F}{\partial t_1^2} - W|F|^2 F e^{-2\bar{\alpha}y_2} = 0, \tag{16}$$

where $K_2 \equiv \partial^2 K/\partial\omega^2$, and

$$W = -\kappa_{13}\int_{-\infty}^{\infty} dz|\zeta(z)|^4 \int_{-\infty}^{\infty} dv f(v)\frac{\zeta(z)\Omega_c a_{32}^{*(2)} + (\omega + d_{21})(2a_{11}^{(2)} + a_{22}^{(2)})}{|\zeta^2(z)\Omega_c|^2 - (\omega + d_{21})(\omega + d_{31})} \Big/ \int_{-\infty}^{\infty} dz|\zeta(z)|^2, \tag{17}$$

and $\alpha = \text{Im}(K) = \varepsilon^2\bar{\alpha}$. The explicit expressions of $a_{11}^{(2)}$, $a_{22}^{(2)}$, $a_{32}^{(2)}$ have been given in Appendix C.

Returning to the original variables, Eq. (16) becomes

$$i\left(\frac{\partial}{\partial y} + \alpha\right)U + \frac{c}{2\omega_p n_{\text{eff}}}\frac{\partial^2 U}{\partial x^2} - \frac{K_2}{2}\frac{\partial^2 U}{\partial\tau^2} - W|U|^2 U = 0, \tag{18}$$

where $\tau = t - y/v_g$ and $U = \varepsilon F e^{-\alpha y}$. Equation (18) is of the form of nonlinear Schrödinger (NLS) equation, but has complex coefficients and hence is not integrable generally. If a nonlinear localized pulse is produced, it may be highly unstable during propagation. However, if a realistic set of system parameters under some conditions can be found so that the imaginary part of the coefficients can be much smaller than their real part, it is possible to obtain a shape-preserving soliton solution that can propagate for a rather long distance without significant distortion. In fact, such parameter set can indeed be found near the EIT transparency window (see below), so the imaginary parts of the coefficients are very small. In this way Eq. (18) can be written into the dimensionless form

$$i\frac{\partial u}{\partial s} + \frac{\partial^2 u}{\partial\sigma^2} + 2u|u|^2 = id_0 u + d_1\frac{\partial^2 u}{\partial\xi^2}, \tag{19}$$

where $s = -z/(2L_D)$, $\sigma = \tau/\tau_0$, $\xi = x/R_\perp$ and $u = U/U_0$. $L_D = \tau_0^2/\tilde{K}_2$ is the characteristic dispersion length, $R_\perp$ is the beam radius in x-direction and $U_0 = 1/\tau_0\sqrt{\tilde{K}_2/\tilde{W}}$ is typical Rabi frequency of the probe field, with $\tilde{K}_2$ and $\tilde{W}$ denoting respectively the real parts of K_2 and W. In Eq. (19), $d_0 = L_D/L_A$ and $d_1 = L_D/L_{\text{diff}}$ are two dimensionless coefficients, with $L_A = 1/2\alpha$ the characteristic absorption length and $L_{\text{diff}} = \omega_p n_{\text{eff}} R_x^2$ the characteristic diffraction length, respectively. Under the condition $d_0, d_1 \ll 1$, Eq. (19) reduces to an integrable NLS equation, which allows multi-soliton solutions. A single soliton solution reads

$$u = 2\beta\,\text{sech}\,[2\beta(\sigma - \sigma_0 + 4\delta s)]\exp[-2i\delta\sigma - 4i(\delta^2 - \beta^2)s - i\phi_0], \tag{20}$$

where β, δ, σ_0 and ϕ_0 are real free parameters that determine the amplitude (also width), propagating velocity, initial position, and initial phase of the soliton, respectively. Taking $\beta = 1/2$, $\delta = \sigma_0 = \phi_0 = 0$, we have $u = 2\beta\,\text{sech}\exp(is)$; or in terms of Rabi frequency

$$\Omega_p = \frac{1}{\tau_0}\sqrt{\frac{\tilde{K}_2}{\tilde{W}}}\,\text{sech}\left[\frac{1}{\tau_0}(t - \frac{y}{\tilde{v}_g})\right]\exp\left[i\tilde{K}_0 y + i\frac{y}{2L_D}\right], \tag{21}$$

#180953 - $15.00 USD Received 30 Nov 2012; revised 13 Jan 2013; accepted 15 Jan 2013; published 22 Feb 2013

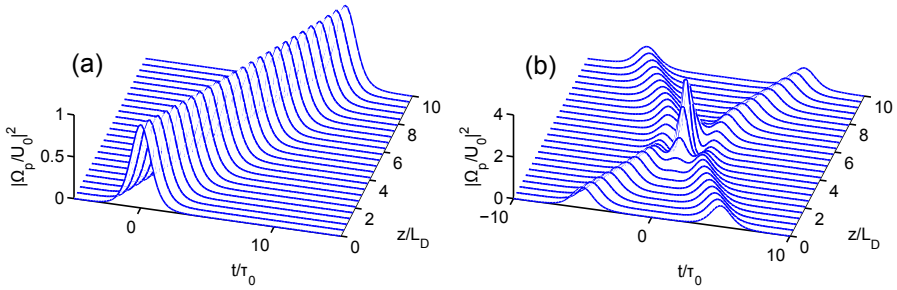

Fig. 5. (a) The three-dimensional plot of the wave shape $|\Omega_p/U_0|^2$ as a function of z/L_D and t/τ_0. The solution is numerically obtained from Eq. (14) with full complex coefficients taken into account. The values of parameters are given in the text. (b): The interaction between two identical bright solitons.

with $\tilde{K}_0 = \mathrm{Re}(K_0)$. Equation (21) describes a bright soliton traveling with velocity $\tilde{v}_g = \mathrm{Re}(v_g)$.

We now consider a practical example for the formation of the optical soliton given above. We choose ^{87}Rb D_1-line transition, with system parameters given by $\kappa_{13} = 1.0\times10^9$ cm^{-1}s^{-1}, $\Delta_2 = 2.5\times10^5$ s^{-1}, $\Delta_3 = 5.9\times10^7$ s^{-1} and slot width $2a = 10$ nm. In this case, the coefficients in Eq. (21) are $K_2 = (1.59+0.14i)\times10^{-14}$ cm^{-1}s^{-2} and $W = (5.1+0.36i)\times10^{-15}$ cm^{-1}s^{-2}. We see that the imaginary parts of these coefficients are indeed much smaller than their corresponding real parts. The physical reason of so small imaginary parts is due to the quantum interference effect induced by the control field, by which the role of population and coherence decay rates for the propagation of the soliton is largely suppressed. When taking $\tau_0 = 1.5\times10^{-7}$ s, $R_x = 0.05$ cm we have the characteristic lengths $L_D = 1.4$ cm, $L_A = 38.4$ cm and $L_{\mathrm{diff}} = 107$ cm, which ensure the validity of neglecting absorption and diffraction of the probe pulse when propagating a distance not much larger than the dispersion length, i.e. $d_0 \ll 1$ and $d_0 \ll 1$ is satisfied. With these parameters we obtain the group velocity $V_g = 1.6\times10^{-5}c$. Consequently, the optical soliton obtained travels with an ultraslow propagating velocity in the system.

The input power for generating the ultraslow optical soliton may be estimated by calculating Poyntings vector. The average flux of energy over carrier-wave period is $\bar{P}/S_0 = (\bar{P}_{max}/S_0)\mathrm{sech}^2[(t-z/\tilde{V}_g)/\tau_0]$ with the peak power $\bar{P}_{max} = 2\varepsilon_0 c n_p S_0 (h/p_{31})^2 \tilde{K}_2/(\tilde{W}\tau_0^2)$. Here, $n_p = n_{\mathrm{neff}} + c\tilde{K}_0/\omega_p$ is the refractive index and S_0 is the cross section area of the probe beam. With the values of coefficients given above, we obtain $\bar{P}_{\max} = 1.19\ \mu$W. Thus, very low input power is needed for generating the ultraslow optical soliton in the slot waveguide system.

In order to make a further confirmation of the soliton solutions and check their stability, a numerical simulation is carried out. Shown in Fig. 5(a) is the three-dimensional plot for the wave shape $|\Omega_p/U_0|^2$ as a function of z/L_D and t/τ_0. The initial condition of the simulation is given by $\Omega_p(0,\sigma) = U_0\mathrm{sech}(t/\tau_0)$. We see that the amplitude of the soliton undergoes only a slight decrease and its width undergoes slight increase due to the influence of the small imaginary parts of the coefficients. The properties of collision between two ultraslow optical solitons are also investigated numerically by taking $\Omega_p(0,\sigma) = U_0\mathrm{sech}(t/\tau_0-5)+U_0\mathrm{sech}(t/\tau_0+5)$ as the initial condition without any approximation. As time goes on, they collide, pass through, and depart from each other, as shown in Fig. 5(b). The two solitons recover their initial waveforms after the collision.

#180953 - $15.00 USD Received 30 Nov 2012; revised 13 Jan 2013; accepted 15 Jan 2013; published 22 Feb 2013

5. Conclusion

We have investigated the EIT and nonlinear pulse propagation in a Λ-type three-level atomic gas filled in a slot waveguide, in which electric field is strongly confined inside the slot of the waveguide due to the discontinuity of dielectric constant. We have found that the EIT effect can be largely enhanced due to reduction of optical-field mode volume contributed by the waveguide geometry. In comparison with the atomic gases in free space, the EIT transparency window in the slot waveguide system are much wider and deeper, and the Kerr nonlinearity of the probe laser field are much stronger. We have also proved that by using the slot waveguide ultraslow optical solitons via EIT can be produced efficiently with extremely low generation power. The present work opens an avenue to the study EIT-related quantum coherence in nano-sized systems and the results presented may have promising applications for optical information processing and transmission.

Appendix

A. TM-modes of EM field and mode volume in the slot waveguide

For the slot waveguide, the EM field can be divided into transverse electric (TE) and transverse magnetic (TM) parts, i.e. $\mathbf{E}=\mathbf{E}^{\rm TE}+\mathbf{E}^{\rm TM}$ and $\mathbf{H}=\mathbf{H}^{\rm TE}+\mathbf{H}^{\rm TM}$. The confinement and enhancement of EM field near the slot region is contributed by the TM part. By solving Maxwell's equations in the absence of atoms, we can obtain the TM eigenmode solutions with the coordinate system chosen in Fig. 1 as

$$\mathbf{H}^{\rm TM}_{m,\mathbf{k}_\parallel}(\mathbf{r},t)=(\hat{\mathbf{k}}_\parallel\times\mathbf{e}_z)H_{m,\mathbf{k}_\parallel}(z)\,e^{i(\mathbf{k}_\parallel\cdot\mathbf{r}-\omega_m t)}+\text{c.c.}, \tag{22a}$$

$$\mathbf{E}^{\rm TM}_{m,\mathbf{k}_\parallel}(\mathbf{r},t)=\frac{i}{\omega_m(\mathbf{k}_\parallel)\varepsilon_0\varepsilon(z)}[-ik_\parallel H_{m,\mathbf{k}_\parallel}(z)\mathbf{e}_z+\frac{d\,H_{m,\mathbf{k}_\parallel}(z)}{dz}\hat{\mathbf{k}}_\parallel]e^{i(\mathbf{k}_\parallel\cdot\mathbf{r}-\omega_m t)}+\text{c.c.}, \tag{22b}$$

where $\mathbf{k}_\parallel=(k_x,k_y,0)$ (k_x, k_y are arbitrary real numbers) is the wavevector in the xy plane, $\hat{\mathbf{k}}_\parallel=\mathbf{k}_\parallel/|\mathbf{k}_\parallel|$ and $\mathbf{e}_z$ are respectively the unit vectors in the $\mathbf{k}_\parallel$- and z-directions, $\omega_n(\mathbf{k}_\parallel)$ is the eigenfrequency with $m=1,2,3\cdots$, and $\varepsilon(z)\equiv n^2(z)$ is dielectric function with $n(z)$ (refractive index) taking the value n_S for $|z|<a$, n_H for $a<|z|<b$, and n_C for $|z|>b$ (see Fig. 1).

The function $H_{m,\mathbf{k}_\parallel}(z)$ in Eq. (22) satisfies the equation

$$\frac{d^2}{dz^2}H_{m,\mathbf{k}_\parallel}(z)+\left[\left(\frac{\omega}{c}\right)^2 n^2(z)-k_\parallel^2\right]H_{m,\mathbf{k}_\parallel}(z)=0, \tag{23}$$

with the boundary conditions $H_{m,\mathbf{k}_\parallel}(z)$, $dH_{m,\mathbf{k}_\parallel}(z)/dz$ being continuous at the interfaces $z=\pm a,\pm b$. For guided modes, an additional condition $H_{m,\mathbf{k}_\parallel}(z)\to 0$ for $z\to\pm\infty$ is also required. Then one obtains [19]

$$H^{\rm TM}_{m,\mathbf{k}_\parallel}(z)=\begin{cases}\cosh(\gamma_{Sm}z), & |z|<a\\ C_m\cos[\kappa_{Hm}(|z|-a)]+D_m\sin[\kappa_{Hm}(|z|-a)], & a<|z|<b\\ E_m\exp[-\gamma_{Sm}(|z|-b)], & |z|>b\end{cases} \tag{24}$$

where $C_m=\cosh(\gamma_{Sm}a)$, $D_m=[n_H^2\gamma_{Sm}/(n_S^2\kappa_{Hm})]\sinh(\gamma_{Sm}a)$, $E_m=\{\cosh(\gamma_{Sm}a)\cos[\kappa_{Hm}(b-a)]+[n_H^2\gamma_{Sm}/(n_S^2\kappa_{Hm})]\sinh(\gamma_S a)\sin[\kappa_{Hm}(b-a)]\}$, with $\kappa_{Hm}=[n_H^2\omega_m^2(\mathbf{k}_\parallel)/c^2-k_\parallel^2]^{1/2}$ and $\gamma_{Sm}=[k_\parallel^2-n_S^2\omega_m^2(\mathbf{k}_\parallel)/c^2]^{1/2}$. The eigenvalue $\omega_m(\mathbf{k}_\parallel)$ is determined by the equation

$$\tan\left[\kappa_{Hm}(b-a)-\arctan\left(\frac{\gamma_{Sm}n_H^2}{\kappa_{Hm}n_S^2}\right)\right]=\frac{\gamma_{Sn}n_H^2}{\kappa_{Hm}n_S^2}\tanh(\gamma_{Sm}a). \tag{25}$$

#180953 - $15.00 USD Received 30 Nov 2012; revised 13 Jan 2013; accepted 15 Jan 2013; published 22 Feb 2013

In fact, the eigenfrequency ω_m depends only on $k_\parallel = (k_x^2 + k_y^2)^{1/2}$, i.e. $\omega_m = \omega_m(k_\parallel)$. Obviously, the guided eigenmodes given above propagate in the *xy*-plane but confined basically in the slot region.

Using the formula $U = \frac{1}{2}\int \mathrm{d}^3 r \left(\varepsilon \mathbf{E}^2 + \mu \mathbf{H}^2\right)$ with U being EM-field energy and ε and μ ($= \mu_0$) being respectively the permittivity and permeability, we obtain the second-quantization form of the TM part

$$\mathbf{E}^{\mathrm{TM}}(\mathbf{r},t) = \sum_{k_x,k_y}\sum_{m=1}^{\infty} \sqrt{\frac{\hbar\omega_m}{2\varepsilon_0 V_m}}\, \mathbf{u}_{m,\mathbf{k}_\parallel}(z)\, \hat{a}_m(\mathbf{k})\, e^{i(\mathbf{k}_\parallel\cdot\mathbf{r}-\omega_m t)} + \mathrm{h.c.}, \tag{26a}$$

$$\mathbf{H}^{\mathrm{TM}}(\mathbf{r},t) = \sum_{k_x,k_y}\sum_{m=1}^{\infty} \sqrt{\frac{\hbar\omega_m}{2\varepsilon_0 V_m}}\, (\hat{\mathbf{k}}_\parallel \times \mathbf{e}_z)\frac{\varepsilon_0 c}{\sqrt{N_m}} H_{m,\mathbf{k}_\parallel}(z)\, \hat{a}_m(\mathbf{k})\, e^{i(\mathbf{k}_\parallel\cdot\mathbf{r}-\omega_m t)} + \mathrm{h.c.}, \tag{26b}$$

where $\mathbf{u}_{m,\mathbf{k}_\parallel}(z) = \{c/[\sqrt{N_m}\omega_m n^2(z)]\}[\mathbf{e}_z k_\parallel H_{m,\mathbf{k}_\parallel}(z) + i\hat{\mathbf{k}}_\parallel dH_{m,\mathbf{k}_\parallel}(z)/dz]$ is the mode function with $\int_{-\infty}^{\infty} dz|\mathbf{u}_{m,\mathbf{k}_\parallel}(z)|^2 = V_m$, $\hat{a}_m(\mathbf{k})$ and $\hat{a}_m^\dagger(\mathbf{k})$ are creation and annihilation operators of TM photons. In our present study, we assume that the photon numbers in both control and probe fields are much larger than one, so $\hat{a}_m(\mathbf{k})$ and $\hat{a}_m^\dagger(\mathbf{k})$ are taken as dimensionless numbers with $\hat{a}_m(\mathbf{k}) = a_n(\mathbf{k})$ and $\hat{a}_m^\dagger(\mathbf{k}) = a_m^*(\mathbf{k})$.

The quantity V_m appeared in Eq. (26) is the (effective) mode volume given by

$$V_m = S\Bigg\{\frac{1}{2\gamma_{Sm}}\left[\sinh(2\gamma_{Sm}a) + 2E_m^2\right] + \frac{a}{2} + (C_m^2 + D_m^2)(b-a) + \frac{1}{2\kappa_{Hm}}(C_m^2 - D_m^2)\sin[2\kappa_{Hm}(b-a)]\Bigg\}/N_m, \tag{27a}$$

$$N_m = \omega_m^2/(cP)^2, \tag{27b}$$

where S is the transverse area of the waveguide in the *xy*-plane, and $P = (k_\parallel^2 + \gamma_S^2)[\sinh(2\gamma_{Sm}a) + 2E_m^2]/(2\gamma_S n_S^4) + n_H^2\omega_m^2(C_m^2 + D_m^2)(b-a)/c^2 + C_m D_m \omega_m^2 \cos[2\kappa_H(b-a)]/(4c^2\kappa_{Hm}n_H^2) + \omega_m^2(C_m^2 - D_m^2)\sinh[2\kappa_H(b-a)]/(4c^2\kappa_{Hm}n_H^2)$.

B. TM-modes and mode volume of EM field without the slot

For conventional slab waveguide (i.e. the waveguide shown in Fig. 1 but with the slot width $2a = 0$), the TM-modes of the EM field have the same form of Eq. (22), but here $n(z)$ takes the values n_H for $|z| < b$, and n_C for $|z| > b$, we have

$$H_{m,\mathbf{k}_\parallel}^{\mathrm{TM}}(z) = \begin{cases} \sin\phi_m \exp\left(\dfrac{z+b}{2b}\psi_m\cos\phi_m\right), & z < -b \\ \cos\left(\psi_m \dfrac{z}{b}\sin\phi_m\right), & -b < z < b \\ \sin\phi_m \exp\left(\dfrac{b-z}{2b}\psi_m\cos\phi_m\right), & z > b \end{cases} \tag{28}$$

where $\phi_m = (n_H^2\omega_m^2(\mathbf{k}_\parallel)/c^2 - k_\parallel^2)^{1/2}L$ and $\psi_m = (2b\omega_m/c)(n_H^2 - n_C^2)^{1/2}$. The eigenvalue $\omega_m(\mathbf{k}_\parallel)$ is determined by the equation $\psi_m \sin\phi_m = m\pi - 2\phi_m$ ($m = 1, 2, 3, \cdots$). The second-quantization

#180953 - $15.00 USD Received 30 Nov 2012; revised 13 Jan 2013; accepted 15 Jan 2013; published 22 Feb 2013

form of the EM field reads

$$\mathbf{E}^{\mathrm{TM}}(\mathbf{r},t)=\sum_{k_x,k_y}\sum_{m=1}^{\infty}\sqrt{\frac{\hbar\omega_m}{2\varepsilon_0 W_m}}\,\mathbf{u}_{m,\mathbf{k}_\parallel}(z)\,\hat{a}_n(\mathbf{k})\,e^{i(\mathbf{k}_\parallel\cdot\mathbf{r}-\omega_m t)}+\mathrm{h.c.}, \tag{29a}$$

$$\mathbf{H}^{\mathrm{TM}}(\mathbf{r},t)=\sum_{k_x,k_y}\sum_{m=1}^{\infty}\sqrt{\frac{\hbar\omega_m}{2\varepsilon_0 W_m}}(\hat{\mathbf{k}}_\parallel\times\mathbf{e}_z)\frac{\varepsilon_0 c}{\sqrt{M_m}}H_{m,\mathbf{k}_\parallel}(z)\,\hat{a}_m(\mathbf{k})\,e^{i(\mathbf{k}_\parallel\cdot\mathbf{r}-\omega_m t)}+\mathrm{h.c.}, \tag{29b}$$

where $\mathbf{u}_{m,\mathbf{k}_\parallel}(z)=\{c/[\sqrt{M_m}\omega_m n^2(z)]\}[\mathbf{e}_z k_\parallel H_{m,\mathbf{k}_\parallel}(z)+i\hat{\mathbf{k}}_\parallel dH_{m,\mathbf{k}_\parallel}(z)/dz]$ is the mode function with $\int_{-\infty}^{\infty}|\mathbf{u}_{m,\mathbf{k}_\parallel}(z)|^2dz=W_m$. $\hat{a}_m(\mathbf{k})$ and $\hat{a}_m^\dagger(\mathbf{k})$ are creation and annihilation operators of TM photons, W_m is the mode volume given by

$$\begin{aligned}W_m=S\big\{&b[2\sin^2\phi_m+\psi_m\cos\phi_m]/(\psi_m\cos\phi_m)\\&+b\sin(2\psi_m\sin\phi_m)/(2\psi_m\sin\phi_m)\big\}/M_m,\end{aligned} \tag{30a}$$

$$M_m=\omega_m^2/(cG)^2, \tag{30b}$$

with $G=[2k_\parallel^2 b\sin^2\phi_m]/(\psi_m\cos\phi_m)+\sin^2\phi_m[\psi_m\cos\phi_m+\psi_m^2/2+\psi_m^2\sin(2\psi_m\sin\phi_m)]/(2b)$.

C. Expressions of $a_{ij}^{(2)}$ appearing in Eq. (17)

$$\begin{aligned}a_{11}^{(2)} &= -i\Bigg\{\Big[i(\Gamma_{12}+\Gamma_{23})-2|\zeta^2(z)\Omega_c|^2\left(\frac{1}{d_{32}}-\frac{1}{d_{32}^*}\right)\Big]\\&\quad\cdot\Big[\frac{(\omega+d_{21}^*)(2\sigma_{11}^{(0)}+\sigma_{22}^{(0)}-1)+\zeta^*(z)\Omega_c^*\sigma_{32}^{(0)}}{|\zeta^2(z)\Omega_c|^2-(\omega+d_{21}^*)(\omega+d_{31}^*)}-\mathrm{c.c.}\Big]\\&\quad+i(\Gamma_{12}-\Gamma_{13})\Big[-\frac{\zeta^*(z)\Omega_c^*}{d_{32}}\frac{(\omega+d_{31}^*)\sigma_{32}^{(0)}+\zeta(z)\Omega_c(2\sigma_{11}^{(0)}+\sigma_{22}^{(0)}-1)}{|\zeta^2(z)\Omega_c|^2-(\omega+d_{21}^*)(\omega+d_{31}^*)}+\mathrm{c.c.}\Big]\Bigg\}\\&\quad\Big/\Big[i(\Gamma_{12}+\Gamma_{21})(\Gamma_{13}+\Gamma_{23})-(2\Gamma_{21}+\Gamma_{12}+\Gamma_{13})|\zeta^2(z)\Omega_c|^2\left(\frac{1}{d_{32}}-\frac{1}{d_{32}^*}\right)\Big],\end{aligned} \tag{31a}$$

$$\begin{aligned}a_{22}^{(2)} &= \frac{i}{\Gamma_{12}-\Gamma_{13}}\Big[\frac{(\omega+d_{21}^*)(2\sigma_{11}^{(0)}+\sigma_{22}^{(0)}-1)+\zeta^*(z)\Omega_c^*\sigma_{32}^{(0)}}{|\zeta^2(z)\Omega_c|^2-(\omega+d_{21}^*)(\omega+d_{31}^*)}-\mathrm{c.c.}\\&\quad-i(\Gamma_{21}+\Gamma_{13})a_{11}^{(2)}\Big],\end{aligned} \tag{31b}$$

$$a_{32}^{(2)} = \frac{1}{d_{32}}\Big[\frac{(\omega+d_{31}^*)\sigma_{32}^{(0)}+\zeta(z)\Omega_c(2\sigma_{11}^{(0)}+\sigma_{22}^{(0)}-1)}{|\zeta^2(z)\Omega_c|^2-(\omega+d_{21}^*)(\omega+d_{31}^*)}-\zeta(z)\Omega_c(a_{11}^{(2)}+2a_{22}^{(2)})\Big]. \tag{31c}$$

Acknowledgments

The authors thanks L. Deng and M. Xiao for useful discussions. This work was supported by NSF-China under Grant numbers 10874043 and 11174080.

#180953 - $15.00 USD Received 30 Nov 2012; revised 13 Jan 2013; accepted 15 Jan 2013; published 22 Feb 2013